

DESIGN AND DEVELOPMENT OF SINGLE-STAGE-TO-ORBIT VEHICLES

A procedure to guide the conceptual design of a single-stage-to-orbit vehicle is presented. Modeling based on historical databases is used to help define plausible flight trajectories and vehicle aerodynamics and to evaluate candidate propulsion cycles. Two conceptual configurations are introduced to examine the sensitivity of vehicle drag, engine cycle selection, and design characteristics on the amount of propellant required to accelerate to orbit. Results show that the choice of the optimum low-speed engine cycle, combined with the ram-scrumjet (supersonic combustion ramjet) at high speed, is very sensitive to the engine air capture and vehicle drag coefficient at transonic speeds. For nominal drag and air capture characteristics, the high thrust and relatively low-efficiency ducted rocket/ram-scrumjet cycle uses about the same weight of propellant as the highly efficient but lower-thrust turbojet ram-scrumjet.

INTRODUCTION

The attractiveness of a single-stage-to-orbit (SSTO) vehicle that could function like a conventional winged aircraft and thereby eliminate the need for a vertical launch complex is self-evident. The feasibility of building and operating such a vehicle, however, must be established. Many formidable challenges must be overcome. In the early phases of a program structured to address these challenges, techniques will be needed to: (1) expedite the identification of good candidate conceptual designs, including the choice of the propulsion system; (2) identify the key technical issues and provide a means for assessing their relative importance; and (3) provide a disciplined procedure to permit a continual assessment of feasibility. Figure 1 shows the sequence of activities involved in the design and development of an SSTO vehicle.

Given a specified mission objective, the available knowledge base is used to generate approximate models for propulsion, aerodynamics, structures, and trajectories that guide the evolution of conceptual designs. The process is iterative and generally proceeds in the order shown in Figure 1 as the models are refined. In the process, the key technical issues and the experiments and analyses needed to resolve those issues are identified. Candidate concepts provide the basis for an intensive research and technology effort that includes tests and analyses of engine components and aerodynamic shapes; design of the entire vehicle structure, fuel tanks, subsystems, etc.; and the selection and development of materials. With this substantial body of knowledge, the initially developed models are replaced, for example, by demonstrated or projected component performances and weights, and the conceptual vehicles are "flown." Optimization techniques are used to identify the best flight path to orbit. Then, when the required and available propellants are matched, the vehicle design is considered "closed."

EQUATION OF MOTION ALONG THE FLIGHT CORRIDOR

A manned SSTO vehicle that can take off and land horizontally has fundamental constraints that guide the development of the model shown in Figure 1. An explanation of the physics underlying these constraints can help to explain the approach. The general equation for the motion of the vehicle along the flight path is

$$m \frac{dU}{dt} = T \cos(\alpha + \delta) - D - mg \sin \theta \quad (1)$$

No general solution to Equation 1 exists, because m , T , D , α , and θ can be functions of U and/or t , and these $f(U)$ or $f(t)$ depend on the vehicle design and flight trajectory. We can gain considerable insight into the design requirements for an SSTO by applying constraints on Equation 1 to yield explicit solutions. We first assume that the terms can be grouped and that any interdependency can be neglected, that is,

$$\int_0^2 dU = U_2 - U_0 = \int_0^2 g \left[\frac{T \cos(\alpha + \delta) - D}{\dot{w}_p} \right] \times \frac{dW}{W} - \int_0^2 g \sin \theta dt \quad (2)$$

where the instantaneous weight is

$$W = mg = W_0 - \int_0^2 \dot{w}_p dt \quad ,$$

\dot{w}_p is the total propellant flow rate in pounds (mass) per second, and the integration can be initialized at $t = 0$

NOMENCLATURE

<i>A</i>	Area	δ	Angle between thrust vector and vehicle axis
C_1-C_7	Constants in Table 1	η_c	Compressor efficiency
C_D	Drag coefficient	η_{cb}	Combustion efficiency
C_p	Specific heat at constant pressure	η_N	Nozzle efficiency
C_T	Thrust coefficient	η_T	Turbine efficiency
<i>D</i>	Drag	θ	Flight path angle
<i>ER</i>	Equivalence ratio	ρ	Density
\mathfrak{F}	Stream thrust = $PA + \rho U^2 A$		
<i>g</i>	Gravitational constant		
g_0	Gravitational constant at sea level	Subscripts	
<i>h</i>	Enthalpy	0	Initial condition, conditions in the freestream
<i>I, I_{SP}</i>	Specific impulse	1	Cowl lip plane
<i>L</i>	Lift	2	Final condition on trajectory
<i>l</i>	Length	3	Conditions at compressor discharge
<i>L/D</i>	Lift-to-drag ratio	4	Conditions following inlet compression
<i>M</i>	Mach number	4'	Conditions following normal shock in inlet
M_D	Design Mach number	5	Conditions at end of combustion
<i>m</i>	Mass	6	Conditions at end of nozzle expansion
<i>O/F</i>	Oxidizer/fuel mass ratio	10	Conditions at turbine inlet
<i>P</i>	Pressure	AB	Airbreather
<i>q</i>	Dynamic pressure = $\rho U^2/2$	a	Point on trajectory
<i>R</i>	Range	b	Point on trajectory, base
<i>r</i>	Distance from center of Earth	c,d,d',	Conditions in nozzle
<i>T</i>	Thrust or temperature	d'',e,j	
<i>t</i>	Time	c	Compressor, cruise
<i>U</i>	Velocity	eff	Effective
U_S	Velocity of circular orbit of Earth	i	Inlet
<i>W</i>	Weight	m	Point on trajectory
W_p	Weight of propellants	max	Maximum value
\dot{w}_a	Air mass flow rate	n	Point on trajectory
\dot{w}_p	Propellant mass flow rate	R	Rocket
<i>x</i>	Axial coordinate	s	Conditions following terminal shock in inlet
<i>Z</i>	Altitude	T	Turbine
Z_S	Altitude of circular orbit	t	Total
α	Angle of attack	x	Axial direction
β	Flow angle		
γ	Ratio of specific heats	Superscript	
		($\bar{}$)	Average value

(thus, $U_0 = 0$). The final condition is at the end of the powered phase, which is then followed by a coast to the desired orbital condition.

The magnitude of U_2 can be closely approximated for a specified orbital requirement, altitude at end of powered flight, and weight/drag characteristics of the vehicle. Here, a nominal condition of a circular polar orbit of 100 nmi is assumed. From Kepler's laws, the velocity required for a circular orbit of the Earth U_S is obtained from

$$U_S = r_0 \left[\frac{g_0}{r_0 + Z_S} \right]^{1/2}. \quad (3)$$

The powered phase of the ascending trajectory must terminate well within the atmosphere, probably in the region of $Z_2 = 170,000$ to $280,000$ ft, which is consid-

erably below Z_S . From this point, an elliptic transfer orbit can be used to define the trajectory of the unpowered phase of the climb to orbit. To a first approximation, if the perigee of a drag-free transfer orbit passing through point S is put at point 2, then the velocity U would equal $U_S(Z_S + r_0)/(Z + r_0)$ according to Kepler's laws. For $Z = 175,000$ ft, $U = 26,103$ ft/s, but to overcome the drag in the unpowered phase, the velocity at point 2 would have to be increased. This increase is a function of the weight at point 2 and the drag characteristics of the vehicle. For a vehicle with $D/qW = 2 \times 10^{-4}$ ft²/lbm, a typical value for an SSTO vehicle, the velocity decrement caused by drag in the transfer orbit would be 497 ft/s. Thus, the velocity at point 2 would be $26,103 + 497 = 26,600$ ft/s. For an easterly orbit with a near-equatorial launch, the requirement would be lessened by the rotational speed of the Earth (1522 ft/s), and U_2 would be 25,078 ft/s. The corresponding

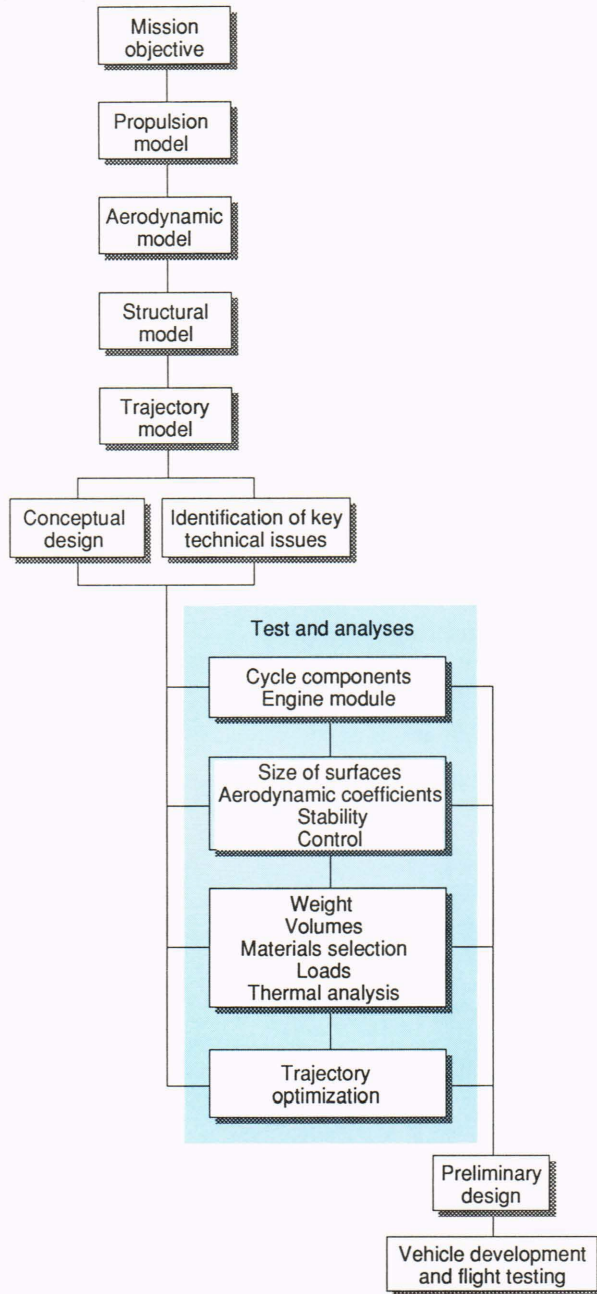


Figure 1. Steps in the design and development of single-stage-to-orbit vehicles.

values for Z_2 located at 280,000 ft would be $U = 25,973$ ft/s, $U_2 = 26,001$ ft/s, and U_2 (easterly) = 24,449 ft/s.

Superficially, one would expect the powered phase to end at the higher altitude: not only is the velocity increment smaller, but the drag is smaller. The amount of propellant required, however, also depends on the specific impulse of the power plant. On the higher trajectory, the amount of air that enters the engine decreases very rapidly as the altitude increases, to the extent that adequate thrust requires the use of an adjunct rocket. The specific impulse of the rocket-airbreather combination is generally lower than that of the airbreather alone.

Thus, it may be possible to arrive at the lower point using airbreathing propulsion with less expenditure of fuel. This subject must be treated parametrically until a more extensive database is available upon which to base the projected performance of airbreathing propulsion at very high speeds. The dynamic pressure $q = \rho U^2/2$ (where ρ is the local air density in pounds [mass] per cubic foot), is a fundamental constraining factor in design. If q is too high, the heat transfer and loads are excessive; if too low, the internal engine pressures are so low that combustion and nozzle expansion losses are unacceptable. Consequently, q will appear as a key parameter in the models that are developed.

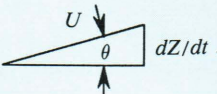
A rigorous evaluation of the integral terms in Equation 2 requires a definition of the engine and aerodynamic characteristics of a particular vehicle and the climb trajectory. Some approximations can be made, however, that closely bound the requirements on the vehicle design and establish the extent of the flight corridor of interest. Table 1 gives expressions for the right-hand term in Equation 2 for three interesting cases. Case 1 can be an excellent representation of the middle portion of an acceleration trajectory, wherein maximum structural loads are a design consideration and the cooling requirements are not excessive. Case 2 permits both of the following: blending of a low-altitude climb with the constant q portion; and/or the constant q portion with a desired end of powered flight condition. Case 3 is a simple method of flying following takeoff, wherein the constants C_5 and C_6 can be selected to match the thrust-weight and aerodynamic characteristics of the vehicle to yield reasonable flight path angles.

To evaluate $\int (g/U) dZ$, flight trajectories must be specified. The green curves in Figure 2 show realistic trajectories for horizontally launched SSTO vehicles. To minimize the $g \sin \theta dt$ term, the trajectory in the lower-speed regime must be suppressed. Vehicle flutter and engine noise limit the maximum q , however. Takeoff speeds must be high because the wing area must be kept low to minimize drag at hypersonic speeds. Consequently, the acceleration must be high to avoid excessive runway lengths. Figure 2 shows a takeoff speed of 500 ft/s, which corresponds to constant accelerations of 0.518 and 0.389 "g" for runway lengths of 7,500 and 10,000 ft, respectively.

To balance flutter, noise, and performance delicately while operating within the constraints of a realizable flight path angle, a low dZ/dU trajectory segment from takeoff at $U_m = 500$ ft/s is blended into a high dZ/dU segment at $U_n = 1200$ ft/s. This segment is modeled as $Z = 2.035 \times 10^{-2}(U^2 - U_m^2)$, with $Z_n = 24,218$ ft and $\int (g/U) dz = 916.6$ ft/s. The next segment of the trajectory is modeled as $U = 500 + 7.23 \times 10^{-3}Z + 8.95 \times 10^{-7}Z^2$, and from Case 2(a) in Table 1, $\int (g/U) dz = 738.5$ ft/s. This segment is blended into a segment having a constant q of 2000 lbf/ft². The constant q trajectory can then be followed until the heat transfer rates on leading edges become excessive, which here is presumed to occur at $U = 14,000$ ft/s. In this segment, from Case 1 in Table 1, $C_1 = 4.748 \times 10^{-5}$ ft⁻¹ and $\int (g/U) dZ = 112$ ft/s.

Table 1. Closed form solutions for the “gravity” term in the acceleration equation (Eq. 2).

Case	Formula	Constraint	$\int_a^b g \sin \theta dt = \int_a^b (g/U) dZ^*$
1	$q = \text{constant}$	$\rho = \rho_a [\exp C_1 (Z_a - Z)]$ $C_1 = \ln(\rho_b/\rho_a)/(Z_b - Z_a)$	$[2g\rho_a/q \exp(C_1 Z_a)]^{1/2}$ $\times [\exp(C_1 Z_b/2) - \exp(C_1 Z_a/2)]/C_1$
2	(a) $U = C_2 + C_3 Z + C_4 Z^2$ (b) $U = C_2 + C_3 Z + C_4 Z^2$	$C_5^2 = (4C_2 C_4 - C_3^2)$ is positive $C_7^2 = (C_3^2 - 4C_2 C_4)$ is positive	$\frac{2g}{C_5} \left[\tan^{-1} \frac{2C_4 Z_b + C_3}{C_5} - \tan^{-1} \frac{2C_4 Z_a + C_3}{C_5} \right]$ $\frac{g}{C_7} \ln \left[\frac{C_3 - C_7 + 2C_4 Z_b}{C_7 + C_3 + 2C_4 Z_b} - \frac{C_3 - C_7 + 2C_4 Z_a}{C_7 + C_3 + 2C_4 Z_a} \right]$
3	$Z = C_5 + C_6 U^2$	None	$2C_6 g (U_b - U_a)$

*This identity 

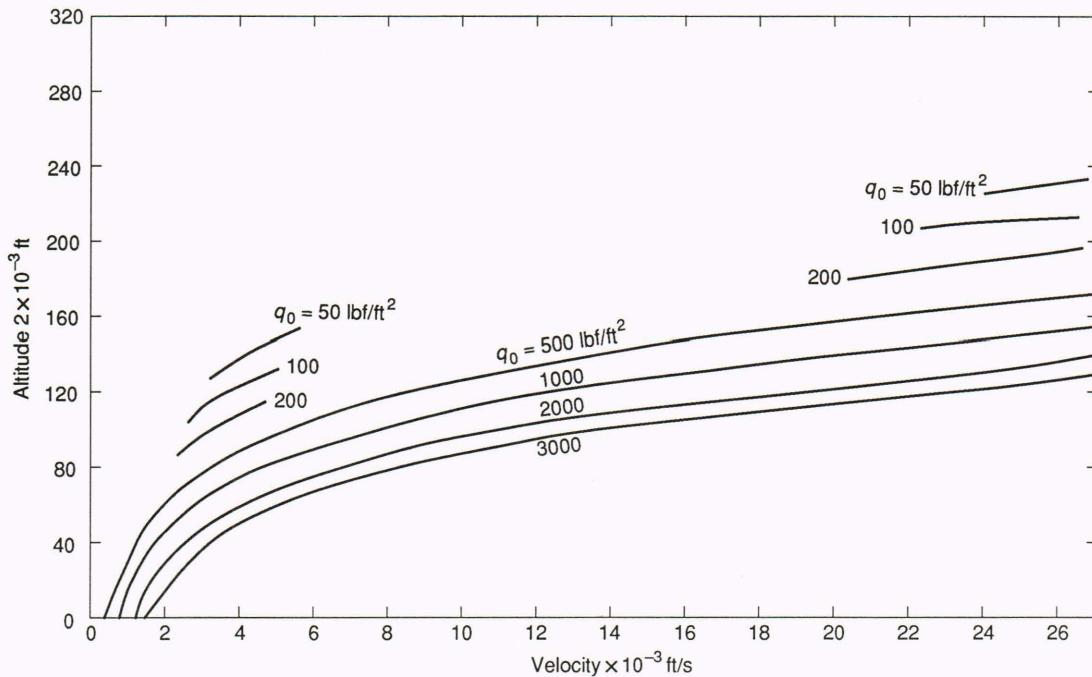


Figure 2. Typical trajectories for single-stage-to-orbit vehicles and shuttle.

Two limiting trajectories are shown for $U > 14,000$ ft/s. The higher trajectory corresponds to a low-drag/low-heat transfer ascent. The q levels reach very low values, however, and the airbreathing propulsion power plant must be augmented by rocket propulsion. For this trajectory segment, $U = -4490 + 0.2059Z - 3.465 \times 10^{-7} Z^2$, and from Case 2(b) in Table 1, $\int (g/U) dZ = 181$ ft/s. The lower trajectory corresponds to the maximum use of airbreathing propulsion (i.e., the minimum

adjunct rocket propulsion), called the reference trajectory. Because the vehicle is at a relatively low altitude, it must “overspeed” to overcome the drag in the unpowered ascent from $Z = 175,000$ ft to $Z = 280,000$ ft. The equation for this trajectory is $U = -39,256 + 0.6647Z - 1.648 \times 10^{-6} Z^2$, and from Case 2(b) in Table 1, $\int (g/U) dZ = 100$ ft/s. Whereas the $\int (g/U) dZ$ is lower for the lower trajectory, the effect of the gravity plus additional drag for overspeed is higher, that is, $(100 +$

497) = 597 ft/s versus 181 ft/s. Which of the two design approaches will prove to require the minimal propellant will ultimately depend on the $[T \cos(\alpha + \delta) - D] / \dot{w}_p$ term in Equation 2.

For comparison, the ascending trajectory for a shuttle (Mission 3A) is shown in Figure 2. Here, a very rapid climb is used to minimize drag and aerodynamic loads. The corresponding value of $\int (g/U) dZ = 4275$ ft/s, however, is 2454 ft/s larger than the higher of the horizontal takeoff airbreathing trajectories.

With the trajectory specified, it is more convenient to rearrange Equation 2 to develop the arguments that dictate the use of airbreathing engines augmented by rockets for an SSTO vehicle, that is,

$$\int_0^2 \frac{dW}{W} = \int_0^2 \frac{\left(1 + \frac{g}{U} \frac{dZ}{dU}\right) dU}{g \frac{T}{\dot{w}_p} \left(1 - \frac{D}{T}\right)}$$

$$= \int_0^2 f(U) dU = \ln \frac{W_0}{W_2} = \ln \frac{1}{1 - \frac{W_P}{W_0}} \quad (4)$$

Here we have assumed that α is small and $\cos \alpha \approx 1$.

For the portions of the trajectory that are governed by the quadratic relationships (Case 2, Table 1),

$$\frac{dZ}{dU} = [C_3 + 2C_4Z]^{-1} \quad (5)$$

and

$$\frac{dZ}{dU} = 2C_6U, \quad (6)$$

and for the $q_0 = \text{constant}$ portion,

$$\frac{dZ}{dU} = \frac{2}{C_1 U_a} \exp\left[\frac{C_1}{2}(Z_a - Z)\right]. \quad (7)$$

The designer's objective is to minimize the required propellant weight fraction W_p/W_0 , which, from Equation 4, means minimizing $f(U)$. By suppressing the trajectory, the numerator has been minimized; thus, the remaining task is to maximize $(T/\dot{w}_p)(1 - D/T)$. Paradoxically, for engines that could be packaged in an SSTO vehicle, those that have the highest T/\dot{w}_p generally have a large D/T . The converse is also true, but engine cycles with very low T/\dot{w}_p can be eliminated from consideration. To explain these effects, a force accounting system must be introduced and cycle analysis must be examined.

FORCE ACCOUNTING

Although the solution to Equation 4 must be independent of which forces on the vehicle are labeled thrust and which are labeled drag, many simplifications accrue with a judicious choice for the force accounting system. Figure 3 will be used to develop this argument. The sketch shows a vehicle powered by an airbreathing engine operating below the inlet design speed, $M_0 < M_D$. Consequently, the shock from the leading edge of the vehicle lies ahead of the engine cowl lip. The air captured in the inlet is in stream tube A_0 . The cross-sectional area labeled A_4 corresponds to conditions following the inlet compression process. The subsequent discussion will argue that the maximum value of A_4 governs the amount of engine air captured at low M_0 . At a higher M_0 , air capture is governed by the position of the forebody wave pattern relative to the cowl lip. Here, the demarcation is, for convenience, set at $M_0 = 3$ to coincide with the flight speed at which the engine transitions from whatever low-speed mode is used to a ram-scrumjet (scrumjet is an acronym for a supersonic combustion ramjet). The elements that comprise the low-speed system all lie within a control volume that is prescribed such that forces can be deduced from change in momentum. These elements are schematically shown as a crosshatched box. The streamline entering and leaving the box is simply a schematic of a splitting of the captured airflow into substreams that could have quite different flow paths but that ultimately mix before passing from the engine.

The expansion of the flow in the exhaust nozzle depends on both the ratio of the total pressure of the expanding gas to the static pressure in the freestream, P_{t_6}/P_0 , and the nozzle geometry. For high P_{t_6}/P_0 , typical of flight at $M_0 > 7$, the nozzle is "underexpanded" (i.e., when the nozzle flow has expanded to the end of the vehicle, $P_6 > P_0$, and the adjustment in pressure in the expanding jet to P_0 occurs beyond the confines of the vehicle). Here, the end of the control volume is the isobaric surface $P_6 = P_e$. In the sectional view of the flow model, the point of intersection of this isobaric surface with the outboard streamline (stream surface) is labeled d. For low P_{t_6}/P_0 , a more complex flow structure exists. In the expansion, the nozzle flow reaches $P_6 = P_0$, well upstream of station e, and then overexpands to $P < P_0$. In general, the overexpansion ends with a compression shock that separates the surface boundary layer. The shock compression raises the pressure back to $P = P_0$ at station j, upstream of the end of the body, and the pressure remains nearly constant from j to e. The end of the control volume here is the upstream isobaric surface $P_6 = P_0$, which may occur within the confines of the cowl. Thus, the control volume for engine thrust accounting ends at d" (inside the cowl), d' (downstream of the cowl exit), or d. The corresponding projected cross-sectional area in the x direction is A_6 . The character of the portion of flow lying between the upstream and downstream isobaric surfaces $P = P_0$ determines the base drag of the vehicle.

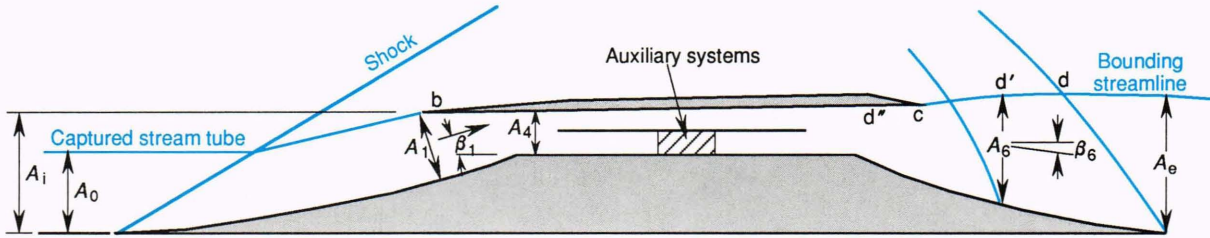


Figure 3. Model for force accounting. (See the Force Accounting section of this article for a fuller discussion of the figure.)

Although the upstream surface of the control volume can be taken in the freestream, it is more conveniently defined as the isobaric surface passing through the cowl lip (point b in Fig. 3). By defining the axial thrust T_x as the “gauge-corrected” change in momentum between stations 1 and 6,

$$T_x = (\rho U^2 A)_6 \cos(\beta_6 + \alpha) - (\rho U^2 A)_1 \cos(\beta_1 + \alpha) - P_0 (A_6 - A_1) \quad (8)$$

When station d (or d') lies downstream of c, a small portion of T_x or pseudo-force $\int_c^d P dA_x$, called “plume drag,” does not act on the body. Thus, a minor correction in T_x must be made to obtain a precise determination of the forces on the body. The axial forces on the remainder of the body are considered as drag. For underexpanded nozzle flows, $A_6 = A_e$, and no base drag on the vehicle exists. For overexpanded flows, a base drag is denoted as

$$D_b = (A_j - A_e) (\bar{P}_{6,j} - P_0) \quad (9)$$

where $\bar{P}_{6,j}$ is the mean pressure on the surface between A_6 and A_j . This force can be large at low flight speeds and will be an important discriminant in the selection of the propulsion scheme at low flight speeds.

A preliminary conceptual design is needed to quantify T and the terms in Equation 8. Cycle analysis is the first step in that process.

CYCLE ANALYSIS

Cycle analysis plays an important role in the development of preliminary vehicle designs. As shown in Figure 4, integral methods are used; that is, a suitable control boundary for the flow path entering the engine is selected, and integral values of the flow variables are defined on convenient elemental surfaces of the control volume. The elemental surfaces are those wall surfaces that are acted upon by (1) the pressure and shear of the captured air flow and (2) the pressure acting on lateral planes representing the freestream, the combustor inlet, the nozzle entrance, and the vehicle base. The equations of motion are solved simultaneously with a suitably defined equa-

tion of state having restrictive assumptions on the thermochemistry. Details on the structuring and operational characteristic of the ramjet performance analysis (RJPA) code used to solve those equations are presented in Ref. 1. The input parameters to the RJPA are treated as independent variables. Modeling, experimental databases, and higher-order analysis are used to reduce the number of parameters and their respective ranges of interest. In addition to generating the engine performance data, cycle analysis provides the input for multi-stream-tube analyses, wherein the flowfield is subdivided into streamlets, and each streamlet is handled by a separate RJPA run. The methodology that uses the RJPA to provide boundary conditions for finite difference methods (CFD's) is discussed in detail in Ref. 2.

The streamline-following technique is an economical approach used to gain insight into the effects of finite rate chemistry in the combustor and nozzle. Solutions from RJPA are used to define the nozzle entrance conditions, and the results serve as revisions to the engine performance from the simpler equilibrium expansion results (see Ref. 3). The subsequent discussion will show how the RJPA and its complementary analytical procedures

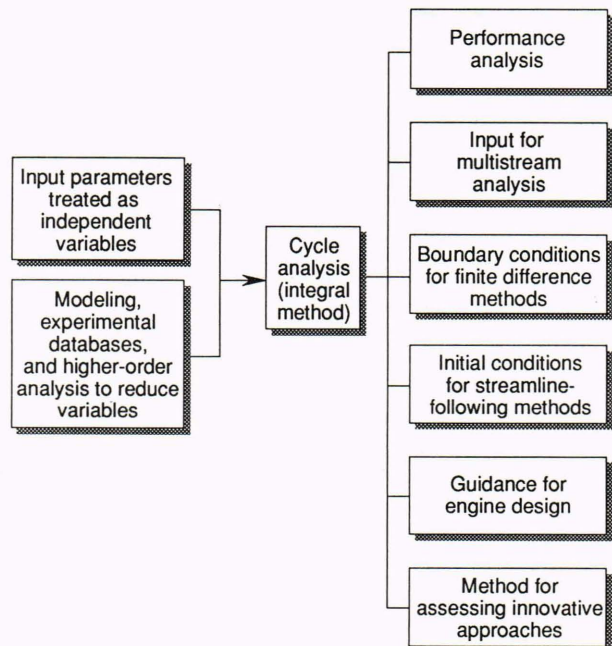


Figure 4. The role of cycle analysis in the development of advanced airbreathing engines.

provide guidance for engine designs and disciplined methods for assessing innovative design approaches.

In the first iteration on the path to a conceptual design, the area ratios of the principal engine components are treated as variables. The results are used as a guide in establishing the preliminary engine lines. Figure 5 will help to explain this procedure. Figure 5A shows the operating modes of the ram-scrumjet engine cycle at low, intermediate, and high flight speeds. Figure 5B shows the desired engine geometries that correspond to the various operating modes on the basis of the cycle analysis results. Air from the freestream is compressed on the vehicle forebody through a series of oblique compression waves and is then turned and further compressed by waves emanating from the cowl. At low speeds the amount of area contraction in the compression process is small; therefore, the engine duct must be as large as practical to permit the capture of an adequate air supply. As the flight speed increases, the amount of contraction increases, and the through-duct must be smaller. Figure 5B (top) shows a typical variation in this desired inlet contraction ratio A_0/A_4 as a function of flight Mach number, M_0 . Although the graph shows a variation in this ratio of about 14 over the range of M_0 , the desired geometric change in A_4 is smaller by perhaps a factor of 3 because of the decrease in the angle of the compression waves on the vehicle forebody as M_0 increases. This folding of the shock waves is manifest in an air capture schedule A_0/A_i for the inlet that increases with M_0 .

Full capture of the inlet (i.e., $A_0/A_i = 1$) means that all the air contained in a stream tube with a cross-sectional area equal to the projected area of the inlet enters the engine. This occurs when the forebody com-

pression waves fall inside the cowl lip. Within limits, the designer can choose M_D , the value of M_0 at which $A_0/A_i = 1$, by placement of the engine cowl lip. A more favorable air capture characteristic can be obtained by selecting a lower M_D , but high inlet efficiency at $M_0 > M_D$ may be difficult to obtain. Movement of the cowl is one attractive option to provide the desired A_0/A_4 and perhaps to obtain optimal wave cancellation in the internal portion of the inlet. While meeting these objectives, however, the movement has only a relatively small impact on A_0/A_i .

Although the flow exiting these external/internal compression inlets can be supersonic at M_0 as low as 3, a subsonic flow at the combustor entrance yields higher performance at $M_0 = 3$ to about $M_0 = 6$. Thus, a normal shock structure (i.e., a shock train) is located at the downstream end of the inlet. A length of duct is required to anchor the shock train, thereby preventing combustor-inlet interaction. This shock-stabilizing section is called an isolator. Two types of internal cross-sectional duct area variations downstream of the isolator can be used in the subsequent heat addition process. In the conventional subsonic ramjet, the duct area is increased before combustion, and a converging-diverging nozzle is added following the combustor. In the dual-mode engines shown in Figure 5, the combustion process begins just downstream of the isolator and continues in a diverging area duct. The heat release and duct area variation are tailored so that the flow accelerates from a subsonic to a sonic or supersonic condition at the combustor exit (see Ref. 4). Thus, the addition of a converging-diverging nozzle is neither necessary nor possible. Figure 5B (middle) shows that the desired combustor

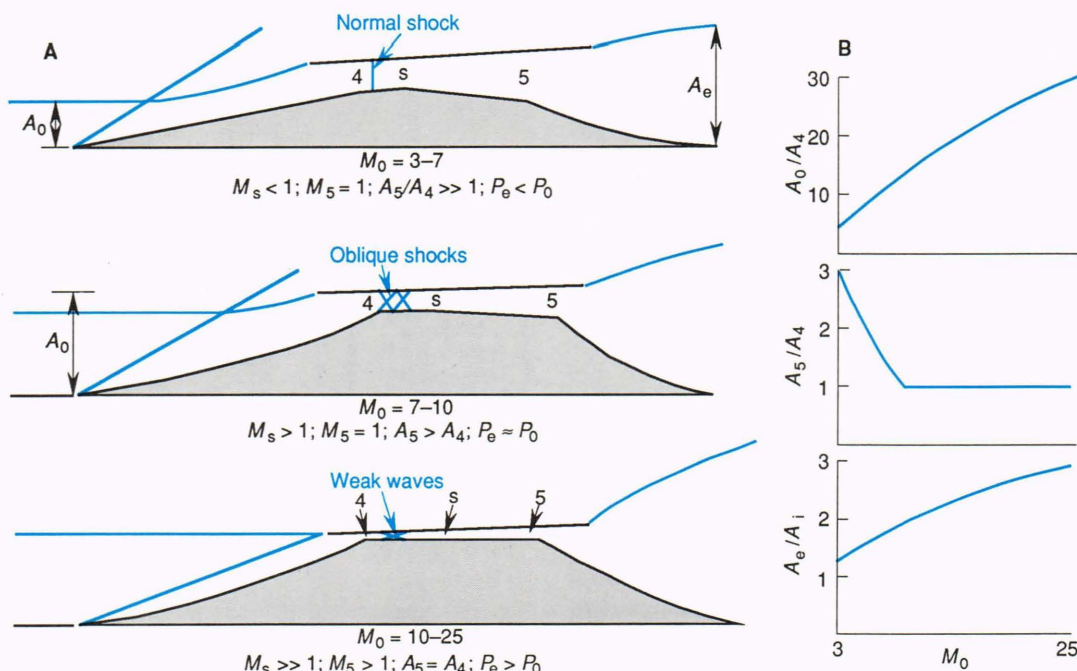


Figure 5. Ram-scrumjet engine cycle. A. Operating modes of the ram-scrumjet engine cycle at low, intermediate, and high flight speeds. B. Desired engine geometries corresponding to various operating modes in A.

area ratio decreases rapidly from $A_5/A_4 > 3$ at $M_0 = 3$ and can be as small as 1 at $M_0 = 7$. Consideration of kinetic losses in the combustor and exhaust nozzle and the maximum permissible pressure rise in the pre-combustion shock train determine the optimum value of A_5/A_4 at $M_0 > 6$. Figure 5A (middle) shows how the shock structure in the isolator accommodates the conditions at M_0 , above the point where $A_5/A_4 = 1$ is first reached. The strength of the shock train decreases, and the mean flow conditions entering and throughout the combustor are supersonic. At very high speeds, the wave structure in the isolator is weak, and the pressure rises are correspondingly small.

The desired nozzle area ratios are shown in Figure 5B (bottom). At M_0 below about 2.5, the exit area would have to be smaller than the inlet to avoid overexpansion of the flow from the engine. Conversely, at high M_0 , a very large area ratio A_6/A_i would be needed to obtain all of the thrust capability of the engine. Therein lies a principal challenge to the vehicle designer, because no practical means to provide the desired variation in A_6/A_i exist. Several approaches are feasible to obtain the variation in A_0/A_4 (in reality A_4/A_i), including movable cowls and adjustable body-side compression ramps. The combustor area ratio variation could be provided either by mechanical means or by adjusting the locations of the fuel injectors.

The next step in the design procedure is an investigation of possible geometric shapes to produce the wave structure to yield the desired inlet compression and contraction ratios. Flow fields are computed for families of compression surfaces with simplifying assumptions on the gas chemistry. These simplifications are removed in the CFD analysis of specified inlet designs. Figure 6 shows typical results for a family of inlets wherein the compression is provided either by a finite number of oblique shocks or on a surface that is shaped to compress the air without shock losses, a so-called isentropic ramp. The wave angles of each set of multiple oblique shock inlets are adjusted to yield maximum efficiency for a given compression ratio. The compression ratio P_4/P_0 is shown as a function of M_0 . Results from the cycle analysis provided the rationale for the values of P_4/P_0 of interest. Significant are the large variation in the desired amount of total flow turning from low to high Mach numbers and the relative insensitivity to the details (i.e., number of shocks) in the compression process.

The required flow turning can be obtained by waves that turn the flow either away from or toward the vehicle axis. To obtain near-coaxial flow at the discharge of the inlet, the outward turning must equal the inward turning. A reasonable strategy is to shape the vehicle forebody to provide one-half the total required turning at the highest operating M_0 and an equal amount of turning toward

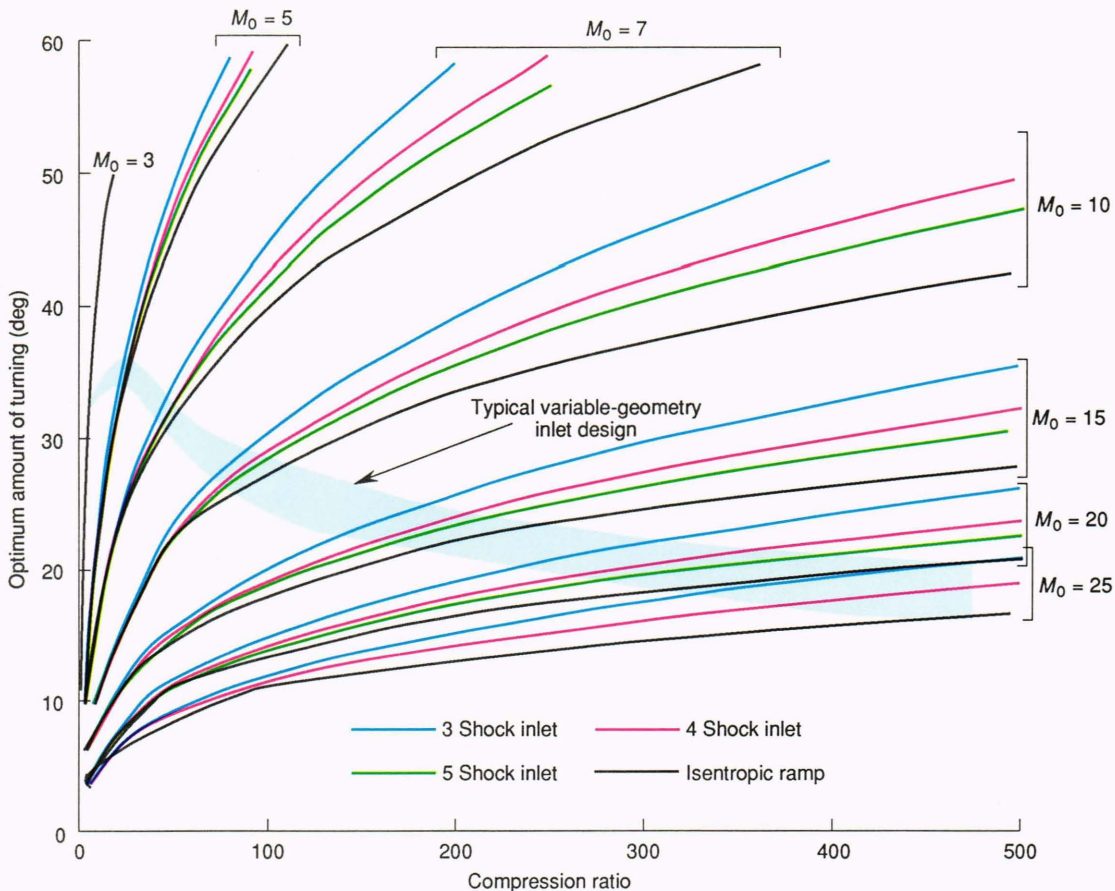


Figure 6. Compression ratios for a family of inlets having optional amounts of turning for flight Mach numbers of 3 to 25.

the vehicle axis from the engine cowl surfaces. From Figure 6, this would suggest a forebody design with 8° to 11° of outward turning. To obtain the larger outward turning at lower M_0 , several options have been considered: (1) adjustable compression ramps on the body side; (2) rotating cowls; (3) adjustable sidewall compression surfaces; (4) a translating cowl; and (5) multipurpose struts that can be inserted to produce additional lateral compression and to serve as in-stream fuel injectors.

All of the techniques introduce mechanical complexities and sealing problems and add weight. Moreover, none are exempt from generating unwanted distortion in the flow field, and the desired schedule of compression ratio with M_0 can only be approximated.

Given that a particular variable geometry concept is viable, either the direct results from CFD analyses of flow fields or a suitable analytical model can be used to further limit the range of parameters needed to be examined in the cycle analysis. The latter method has considerable merit in the early stages of conceptual design, especially if the model contains features that permit realistic examination of design variables (e.g., M_D). An example of this modeling for $3 \leq M_0 \leq 25$ is:

air capture ratio

$$\begin{aligned} \frac{A_0}{A_i} &= 1 - (M_D - M_0) \\ &\times (0.155 - 0.94 \times 10^{-2}M_D \\ &+ 1.8 \times 10^{-4}M_D^2) \text{ for } M_D < M_0 \\ &= 1 \text{ for } M_D \geq M_0; \end{aligned} \tag{10}$$

inlet contraction ratio

$$\frac{A_0}{A_4} = -3.5 + 2.17M_0 - 0.017M_0^2; \tag{11}$$

inlet compression ratio

$$\frac{P_4}{P_0} = -8.4 + 3.5M_0 + 0.63M_0^2. \tag{12}$$

The independent variable in Equation 10 is M rather than U as in the preceding discussion, since the inlet parameters are, in part, governed by the wave structure in the flow field, which is Mach-number dependent. Conversely, the more fundamental parameter for the flight mechanics, engine thrust, and drag is U .

By using the modeling of Equations 10 through 12 and an assumed 1% loss in total enthalpy from the inlet surfaces by radiation to space, we can calculate the mean flow conditions at the combustor inlet. Table 2 lists values of these conditions for the lower reference trajectory shown in Figure 2. Although P_4/P_0 increases by a factor of about 60 over the range of M_0 , the static pressures at the isolator entrance vary by only a factor of 6. Additional pressure rises in the shock train depend on the engine fuel/air equivalence ratio ER and the combustor area ratio A_5/A_4 . Maximum rises occur at Mach 6 and 7 and can be as high as a factor of 5 to 10 (i.e., local pressure can be in the 100- to 200-psia range). The structural design of the engine is governed by these conditions. Maximum heat transfer, and hence the maximum cooling requirements, depend primarily on the driving enthalpy and local dynamic pressure. The combined effects are most severe in the Mach 15 to 20 range. The mean static temperature T_4 increases by about 200°R for a unit increase in M_0 and reaches a level ($T_4 > 4000^\circ\text{R}$) where dissociation of oxygen becomes significant at about $M_0 = 17$ to 20. Within the boundary layer, the temperature can be significantly higher, especially at high M_0 . For $M_0 < 9$, the static temperature before the shock train is below 1800°R, which is the minimum temperature required to auto-ignite hydrogen. This suggests the need for an ignition source at low M_0 ; with ignition, considerable heat will have to be released to ensure the establishment of a precombustion shock structure to raise the temperature throughout the flow. The mean values of M_4 increase monotonically with M_0 , and the ratio of M_4/M_0 decreases from about 0.5 at $M_0 = 3$ to 0.3 at $M_0 = 25$. The velocity decrements U_0 through U_4 increase from about 870 ft/s at $M_0 = 3$ to about 1660 ft/s at $M_0 = 25$. The velocities in the combustor, however, remain very high at high M_0 , which means that

Table 2. Conditions in the freestream and the combustor inlet in a typical ram-scamjet engine.*

M_0	Freestream conditions						Isolator entrance conditions					
	Z_0 (ft)	P_0 (psia)	T_0 (°R)	U_0 ft/s	q_0 (lbf/ft ²)	$h_{t_0}^\dagger$ (BTU/lbm)	M_4	A_0/A_4	P_4/P_0	P_4 (psia)	T_4 (°R)	U_4 (ft/s)
3	47950	1.868	390.0	2904	1694	133.3	1.529	2.86	7.8	14.51	744	2034
4	57480	1.183	390.0	3872	1910	264.3	1.945	4.91	15.7	18.57	930	2885
5	65720	7.978 ⁻¹	390.0	4840	2011	432.8	2.363	6.92	24.9	19.86	1102	3799
6	73300	5.569 ⁻¹	394.0	5839	2020	646.7	2.767	8.91	35.3	19.65	1279	4770
7	80077	4.049 ⁻¹	397.7	6844	2000	902.3	3.143	10.85	47.0	19.03	1451	5757
10	95500	1.984 ⁻¹	406.1	9879	2000	1918.2	4.143	16.49	89.6	17.78	1958	8744
15	114250	8.577 ⁻²	424.8	15155	1945	4561.0	5.502	25.23	185.9	15.94	2880	13908
20	137760	3.194 ⁻²	460.8	21040	1287	8824.6	6.650	33.11	313.6	10.02	4074	19648
26.9	178210	6.759 ⁻³	480.5	28865	425.8	16629.8	7.688	40.12	472.9	3.20	5187	27205

*Lower reference airbreathing trajectory in Figure 2.

† $h = 0$ at 536.7°R.

the mixing and combustion must be extremely rapid. For example, at $M_0 = 20$, the residence time in a 5-ft-long duct would be only $10 \mu\text{s}$.

With conditions at station 4 specified, engine cycle analysis is used to parametrically examine the mean flow conditions and geometric requirements at the combustor entrance and exit and at the end of the nozzle expansion. In the early stages of the evolution of the conceptual design, however, the problem of nonideal nozzle expansion must be addressed. The results shown in Figure 7 explain the problem. The ratio of nozzle exit to free stream pressure P_6/P_0 is shown as a function of flight Mach number for three values of A_6/A_i : 1.0, 1.75, and 2.5. Pressure ratios increase with M_0 . When $P_6/P_0 < 1$, the nozzle flow overexpands, which produces base drag; when $P_6/P_0 > 1$, the full potential of the engine exhaust to produce thrust cannot be realized. A compromise in the choice of A_6/A_i must be made in the design of a vehicle that operates over a wide range of M_0 . Cycle analysis together with trajectory calculations help to determine the optimum value for a vehicle that accelerates from takeoff to a prescribed M_0 . As shown by the black curve in Figure 7, A_6/A_i should be about 1.75 for an SSTO airbreathing engine.

Again, the engine air flow characteristics for low-speed cycle conditions are governed by the geometric limits imposed on A_4 . Considering the practical structural and actuator constraints and limitations on fuel distribution, let us suppose that the geometry can be varied such that A_4 for low-speed engine operation can be 4.92 times larger than at high speed. Moreover, at high speed $A_0 = A_i$, and the values of A_0/A_4 from Table 2 are to be matched. Assuming that an increase in A_4 also results in an increase in A_i (e.g., from outward translation of the cowl), $A_4/A_i = 0.0249$ at $M_0 = 25$ and $A_4/A_i = A_{4\text{max}}/A_i = 4.92(1 + 40.12) = 0.120$ at $M_0 \leq 3$. From Table 2, $A_0/A_4 = 2.86$ at $M_0 = 3$; thus, $A_0/A_i = 2.86 \times 0.120 = 0.342$ at $M_0 = 3$.

For low-speed cycles, the air capture can then be calculated for a desired Mach number at station 4 of the inlet total pressure recovery as specified. The model adopted for total pressure recovery for $0 \leq M_0 \leq 3$ is

$$\frac{P_{t4'}}{P_{t0}} = 1 - 0.0291M_0 - 0.0206M_0^2, \quad (13)$$

where 4' means that the conditions at the end of compression are subsonic. The modeling depended on matching $P_{t4'}/P_{t0}$ at $M_0 = 3$, with the value that would be obtained through a normal shock at M_4 set by Equations 11 and 12 as given in Table 2. With $P_{t4'}/P_{t0}$ given by Equation 13, the limits on A_0/A_i for $M_0 \leq 3$ can be established for low-speed cycles by specifying $M_{4'}$. Two classes of low-speed engines establish the limit curves shown in Figure 8. The first class comprises engines that use rotating machinery to compress the air (e.g., turbojets). In these engines, the Mach number entering the compressor should be low, so $M_{4'} = 0.3$ is taken as the lower bound. The other class uses ejector pumping to compress the air (e.g., ducted rockets). These

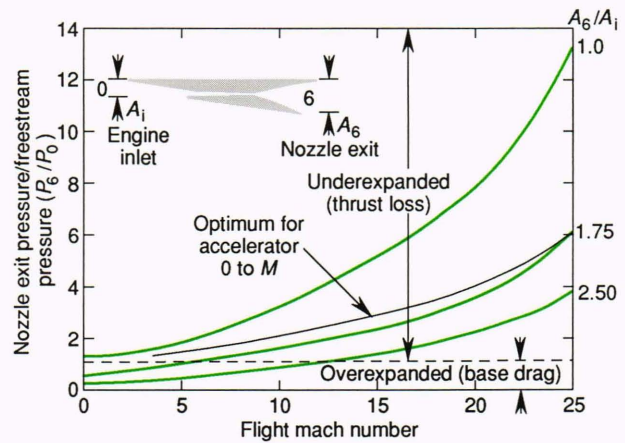


Figure 7. Nozzle exit pressure ratios for three engine geometries ($A_6/A_i = 1.0, 1.75, \text{ and } 2.5$) and for a family of optimal fixed geometries, wherein the engine operates from $M = 0$ to M_0 on the ordinate.

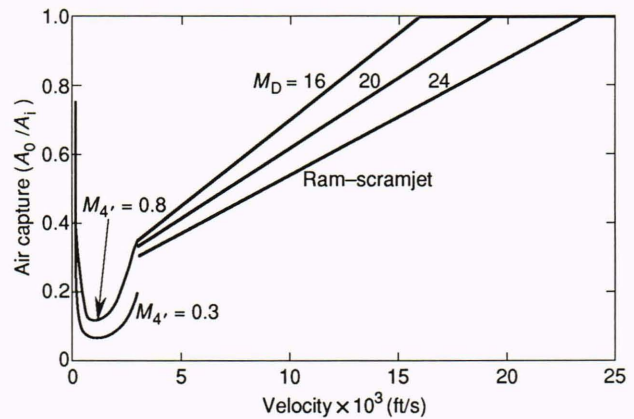


Figure 8. Inlet air capture characteristics.

cycles optimize with high entering Mach numbers so that $M_{4'} = 0.8$. The results shown in Figure 8 are disconcerting to the designer of an accelerator; in the transonic region, the air capture ratios are so low that either the transonic “barrier” cannot be crossed or an enormous amount of fuel would be used to accelerate through the barrier. The only solution is to augment the thrust with rocket propulsion. The rocket can be a tandem system or can be embedded within the airflow path. Curves of A_0/A_i for $M_0 > 3$ calculated from Equation 10 are shown for $M_D = 16, 20, \text{ and } 24$. The subsequent analysis will show that the increased air capture for $M_D = 16$ results in a lower fuel requirement to reach orbit.

With the air capture characteristics defined, the performance for airbreathing cycles can be computed and expressed in terms of the engine specific impulse I_{AB} and thrust coefficient C_{TAB} , which are given as

$$C_{TAB} = T/q_0 A_i = \eta_N \mathfrak{F}_6 \cos \beta_6 - \mathfrak{F}_1 \cos \beta_1 - P_0 \times (A_6 \cos \beta_6 - A_1 \cos \beta_1) / q_0 A_i \quad (14)$$

and

$$I_{AB} = \frac{T}{\dot{w}_p} = \frac{\eta_{cb} C_T U_0 A_i \dot{w}_a}{64.35 A_0 \dot{w}_p} \quad (15)$$

Here, $\eta_N = 0.98$, $\eta_c = 0.95$, and $\dot{w}_p/\dot{w}_a = 0.02917$ *ER* for engine cycles where the total propellant is hydrogen. For cycles where oxygen is part of the propellant, \dot{w}_p/\dot{w}_a includes both the hydrogen and oxygen.

Although the ramjet-scrumjet cycle has the greatest potential for maximizing the denominator of Equation 4 over the range $3 \leq M_0 \leq 25$, other cycles must be considered for $M_0 < 3$. For this study, two limiting cases are examined: the turbojet with a high specific impulse and the ducted rocket with a high thrust coefficient.

The performance of the turbojet cycles was based on an optimal compressor pressure ratio cycle at all flight speeds, without consideration of additional "off-design" losses. The optimum compressor pressure ratio is

$$\frac{P_4}{P_3} = \left(\frac{1}{G + 1} \right) \times \left[\frac{C_{p10} T_{t10}}{C_{p3} T_{t3}} (1 + f)\eta_T + \eta_c + 1 \right]^{\gamma_c/\gamma_c - 1} \quad (16)$$

where $G = (\gamma_c - 1/\gamma_c)(\gamma_T/\gamma_T - 1)$.

Values of $\eta_c = 0.85$, $\eta_T = 0.90$, and $T_{t10} = 3000^\circ\text{R}$ were used in this analysis. Calculations were made for the *ER* corresponding to $T_{t10} = 3000^\circ\text{R}$ with no afterburning and *ER* = 1 with afterburning.

The ducted rocket is simply a variant of the ramjet engine, wherein the propellant that is added to the airstream is a fuel-rich rocket exhaust. The rocket is embedded in the ramjet duct and serves the dual purpose of providing a hot, easily ignited fuel and an ejector to raise the total pressure of the system. The oxidizer-to-fuel ratio of the "rocket" and \dot{w}_p/\dot{w}_a are treated as parameters in the analysis. For the SSTO application, these ratios are varied to minimize the fuel required to accelerate. For the ramjet-scrumjet, the *ER* is also treated as a variable, and the optimum values are used.

Figure 9 shows the computed values of specific impulse for these cycles. The turbojet operating without an afterburner has, by far, the highest I_{SP} , with values decreasing from 12,400 lbf·s/lbm at $M = 0$ to 6218 lbf·s/lbm ($U = 2904$ ft/s) at $M = 3$. With the afterburner, the corresponding values are 5360 and 4770 lbf·s/lbm, respectively. The specific fuel consumptions of 0.290 and 0.579 lbm/lbf·h are low relative to state-of-the-art engines because the assumed turbine inlet temperature of 3000°R is quite high. With the engine sized to meet the $A_{4_{max}}/A_i$ constraint, sea level static thrusts are 48,200 and 36,500 lbf for operation with and without the afterburner, respectively.

The value of $I_{SP} = 418$ lbf·s/lbm for the ducted rocket at $U = 0$ slightly exceeds that for a hydrogen-oxygen rocket. Two branches are shown in Figure 9 be-

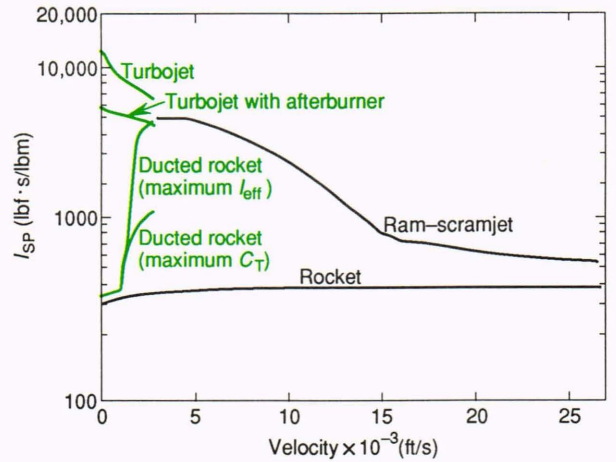


Figure 9. Computed values of specific impulse.

tween $U = 1100$ and 2904 ft/s. The lower branch corresponds to a large \dot{w}_p/\dot{w}_a and the highest C_T that the ducted rocket could produce following the prescribed trajectory without exceeding a 60° climb angle. On the higher branch, the engine is operated at a propellant flow rate and mixture ratio that results in minimum propellant use for the high vehicle drag assumed in this study. Both engines have sufficient thrust to accelerate the vehicle through the transonic "pinch" without requiring rocket augmentation. Some propellant would be saved if the ducted rocket were supplemented by a rocket during transonic pinch, but the savings would not exceed the weight of the adjunct rocket. This ducted rocket can produce up to 175,000 lb of thrust at sea level static.

The values of I_{SP} for the ram-scrumjet correspond to an *ER* schedule that results in a minimum fuel requirement for acceleration to orbit. Minor differences in I_{SP} occur at $M_0 > 16$ for the three values of M_D examined (16, 20, and 24), but these differences are imperceptible at the scale shown in Figure 9. Conversely, the effect of altitude on I_{SP} at $M_0 > 16$ is significant. On both trajectories at $M_0 > 16$, oxygen is added in the propellant to obtain maximum I_{SP} . The I_{SP} values for the higher trajectory are lower, however, because the efficiency of the airbreathing engine decreases rapidly at altitudes above 175,000 ft. Indeed, without oxygen addition the engine would not produce thrust greater than drag. In reality, the ram-scrumjet operates as a ducted rocket at very high speeds.

The subsequent analysis will show that either of the turbojet cycles would need the assistance of an adjunct rocket to meet the acceleration requirements for takeoff and to avoid the use of excessive amounts of fuel to accelerate through the transonic region. Selection of the size of the adjunct rocket is a trade-off between the benefits that accrue with a large thrust increment and the difficulty in packaging the system, as well as the volume and weight. Sensitivity studies suggest that a design producing 600 lbf/ft² of engine frontal area is about optimum. For these vehicles with $A_i = 100$ ft², the thrust requirement is therefore 60,000 lb at sea level. For this study a chamber pressure of 1500 psia and an *O/F*

(O₂/H₂ weight ratio) of 5.29 were assumed, with a “c star” efficiency of 0.95. The resulting throat area is 24.04 in². A curve of the specific impulse of this rocket I_R as a function of U for the reference trajectory is also shown in Figure 9. A trivial increase in I_R would occur on the higher trajectory at $U_0 > 14,000$ ft/s.

Thrust coefficients for the propulsion cycles are shown in Figures 10 and 11. For clarity, portions of the curves at $C_T > 3$ are not shown. The relatively low values of C_T for the turbojet cycle at low speeds (Fig. 10) are apparent. The range of C_T values available in the ducted rocket cycle is quite broad, which permits the opportunity to provide engine thrust in accordance with the drag characteristics of the vehicle. Rocket C_T values decrease monotonically with U since Z increases with U . Had a larger rocket been chosen, C_T values would have been proportionately larger. Figure 11 compares the C_T values for the ram-scrumjet and the rocket. For the lower speeds, the differences in C_T for the different M_D values lead to differences in the required propellant needed to accelerate. At $U > 16,000$ to 18,000 ft/s, the addition of oxygen in the ram-scrumjet can be beneficial.

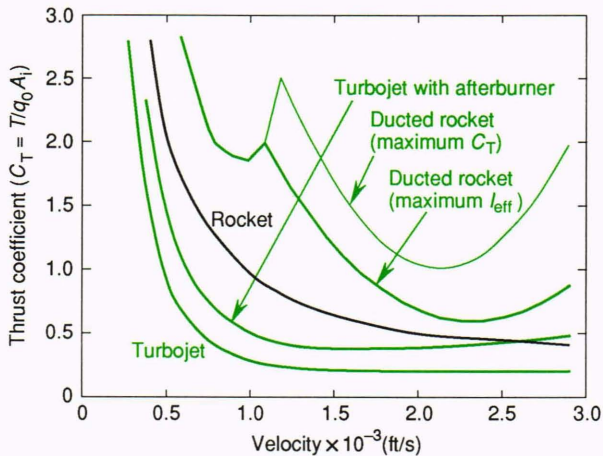


Figure 10. Low-speed engine thrust coefficient.

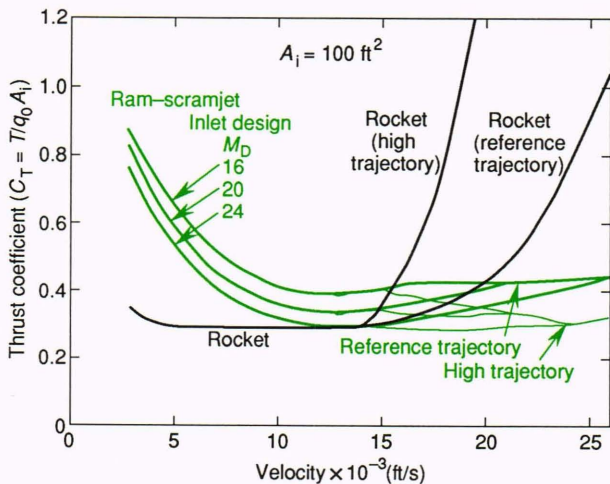


Figure 11. High-speed engine thrust coefficient.

The amount that is added (and therefore the resultant C_T) depends on the trajectory, which is indicated by the branching of the curves in the figure. The rocket C_T curves also branch because the thrust is nearly constant, but q is quite different on the two trajectories.

To complete the trajectory analysis, vehicle drag must be assessed. Since drags are configuration dependent, conceptual vehicle designs must be generated.

CONCEPTUAL DESIGNS

At this point, the rudiments of a database are available to proceed with conceptual designs. The information was the basis for the two generic engine designs shown in Figure 12. Both have maximum inlet capture areas of 100 ft² at Mach 25 and maximum body cross-sectional areas of 175 ft²; one is a two-dimensional planar geometry (PGE), and the other is a so-called axisymmetric sector engine (ASE). Overall vehicle lengths and cross-sectional area distribution were selected on the basis of fuel tank volume requirements and drag considerations. The inlet cowls were set at an $x/l \approx 0.67$, where x is the axial coordinate and l is the fuselage length, since previous studies (see, e.g., Ref. 5) suggested that the engine modules should be at about this location to provide stability and control with low induced drag.

Both inlets are of the external-internal compression type, wherein the flow is turned outboard by the cone sector (ASE) or wedge (PGE) and then returned coaxially by the straight cowl. In the ASE, the forebody is a 1.5-in.-radius, 5.85° half-angle blunted cone followed by a curved surface that turns the flow outboard, reaching an angle of 10.2° at $x = 1221$ in. A sector angle of 67.8°, a cowl lip radius of 13 ft, and the location of the axis of symmetry were selected to yield the desired air capture ratio and to provide forebody section geometries that include circular fuel tank cross sections with very little wasted space.

To obtain a near-planar compression field in the PGE, a tapered forebody that is flat on the undersurface is required. The initial wedge compression angle is 4.27°, which, with the cowl at $x = 1320$ in., yields a capture height of 78 in. and the desired capture area of 100 ft². The compression surface is curved from $x = 1063$ to 1199 in., where the angle reaches 10°.

To provide the desired cross-sectional area change in the internal ducts and wave cancellation at the shoulder of the innerbody, the respective cowls and cowl flows are translatable. For orbital flight and reentry, the cowls flap close against the vehicle body. Both configurations show interior walls that subdivide the internal flow into individual engine modules. The planform areas of the underbodies are 2425 ft² and 3160 ft² for the ASE and PGE, respectively.

TRAJECTORY ANALYSIS

With the conceptual designs specified, reasonable estimates of vehicle drag can be made. Figure 13 shows drag coefficients based on frontal area determined from relatively simple modeling and historical databases. The nominal drag curve includes a base drag penalty caused

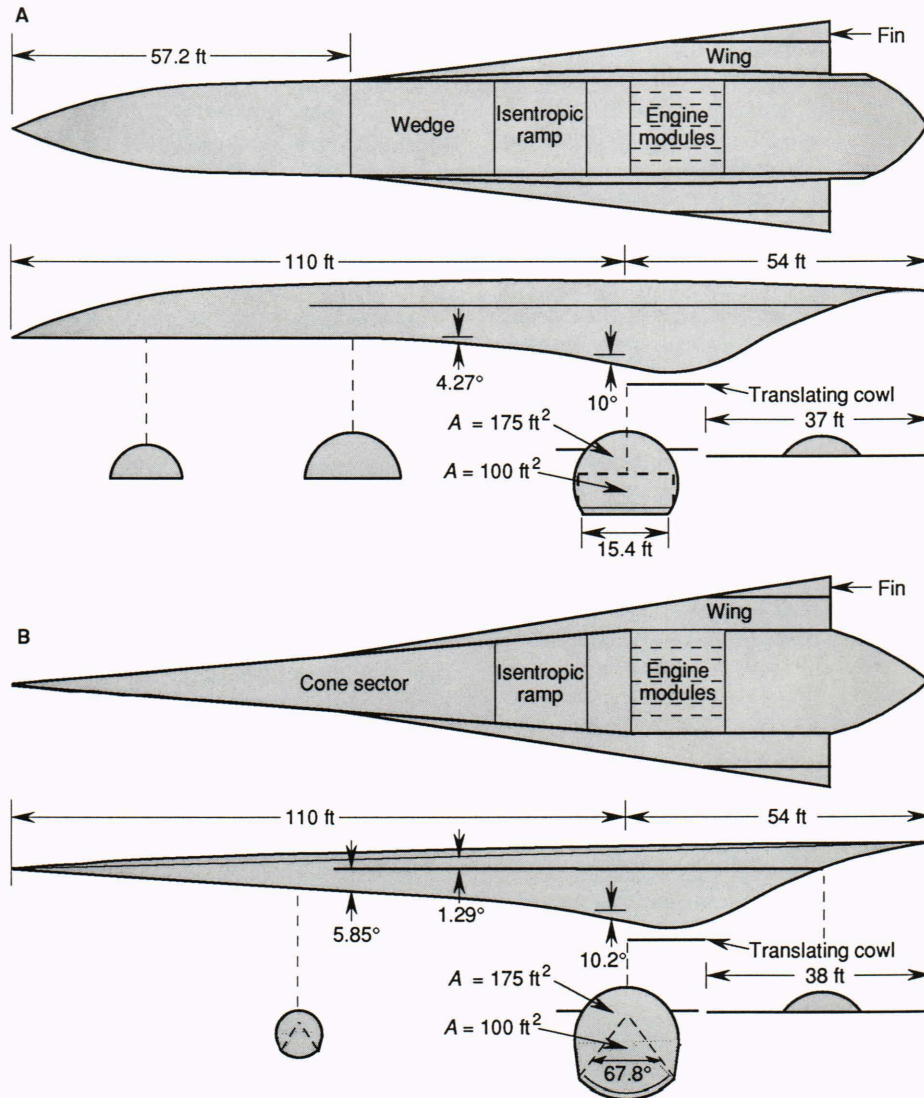


Figure 12. Two schematic engine designs. **A.** Planar geometry engine. **B.** Axisymmetric sector engine.

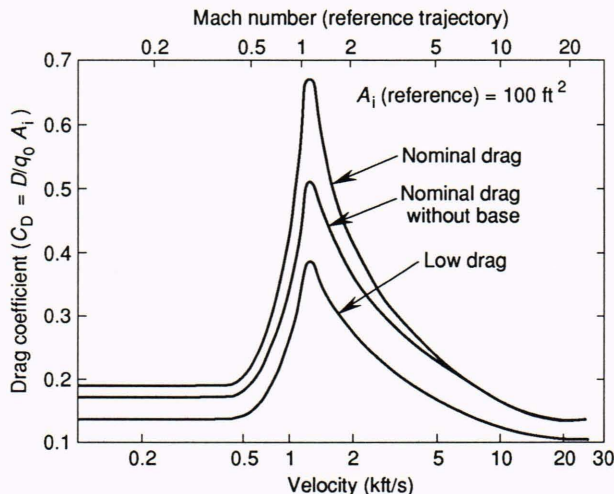


Figure 13. Vehicle drag coefficient based on inlet area.

by overexpansion of the engine exhaust at $M_0 = \leq 7$. If by some means (e.g., external burning) this drag could be eliminated, the significant reductions in C_D would be realized. The lowest curve in Figure 13 is included to assess the benefits that could accrue if an extremely efficient aerodynamic configuration could be designed.

With C_T , C_D , I_{AB} , and I_R defined, we can now integrate Equation 13 to obtain the propellant mass fraction needed to accelerate to orbit. A simple test can be made to determine whether it is beneficial to augment the air-breathing propulsion cycle with a rocket. If

$$\frac{C_D}{C_{TAB}} > 1 - \frac{I_R}{I_{AB}}, \quad (17)$$

then the rocket should be turned on and the denominator of Equation 4 becomes

$$g \frac{T}{\dot{w}_p} \left(1 - \frac{D}{T}\right) = g I_{AB} \left(\frac{C_{TAB} + C_{TR} - C_D}{C_{TAB} + C_{TR} I_{AB}/I_R} \right) \quad (18)$$

Equation 17 also holds for rocket assist before takeoff.

Plots of the integrands of Equation 4 for several engine combinations using the nominal drag and flying the reference trajectory are shown in Figure 14. The propellant required to accelerate to orbit is proportional to the area under the curve. Obviously, engine/vehicle performance at transonic and high hypersonic speed ranges dictates the propellant requirement. For $M_0 > 3$, the engine is the ram-scrumjet without rocket augmentation at high speed. Curves are shown for the three inlet design Mach numbers. Lowering the design Mach number of the inlet leads to savings of fuel. The curves for the lower speed range have been enlarged in Figure 15.

While on the runway, rocket augmentation of the turbojet engine nearly negates the large specific impulse advantage of the turbojet over that of the ducted rocket. To obtain a velocity of 500 ft/s in 10,000 ft, the rocket must be on until velocities of 330 and 432 ft/s are reached for the turbojet with and without the afterburner, respectively. After the rocket acceleration is no longer needed and until it must be turned on transonically, the high specific impulse of the turbojet provides the desired benefit of lower fuel expenditure. At $U = 900$ ft/s, with the basic turbojet, the rocket is turned back on in accordance with the criterion of Equation 17. It remains on until the switch to the ram-scrumjet. With the afterburner, the rocket is on from $U = 1100$ ft/s until $U = 2200$ ft/s. Rocket augmentation is not needed with the ducted rocket cycles. In fact, the ducted rocket can produce up to 175,000 lbf of thrust at sea level static. If desired, the 160,000-lb airplane, powered with a ducted rocket, could be airborne 3500 ft down the runway. Since there is no rocket augmentation, the ducted rocket having maximum I_{eff} has a lower value of the integrand in Equation 4 than the maximum C_T ducted rocket and therefore uses less propellant to accelerate.

Table 3 shows the propellant required to accelerate to Mach 3, $U = 2904$ ft/s, for the four engine cycles. For nominal drag, the ducted rocket operating at maximum I_{eff} consumes slightly less propellant than the afterburning turbojet. Operating the ducted rocket at maximum C_T has no advantage, but the difference is not too great. The basic turbojet cycle uses about 50% more propellant, which provides a rather convincing argument for avoiding the use of low-thrust, high specific impulse cycles for SSTO missions. If the base drag could be canceled or if a very low drag vehicle could be designed, the savings in propellant would be significant, and the use of a higher specific impulse airbreathing engine would become more attractive. Conversely, one can argue that the ducted rocket is an ideal engine choice because of its relative insensitivity to vehicle drag and high thrust-to-weight ratio.

When the propellant weight fractions required to orbit are compared, the differences in propellant fraction are smaller, as indicated in Table 4. Values are shown for the two cycles of interest for the three inlet design Mach

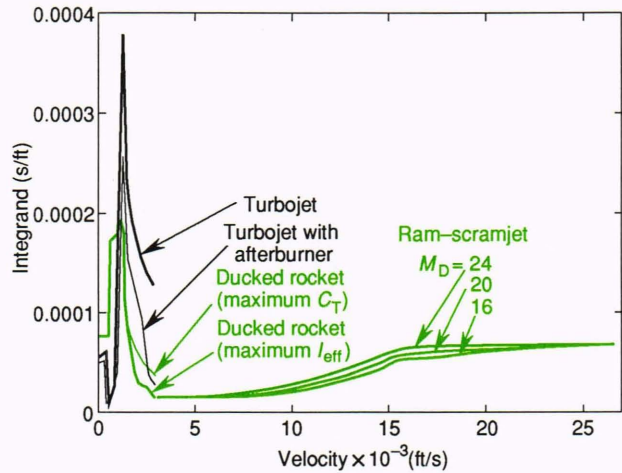


Figure 14. Values of the integrand in Equation 4.

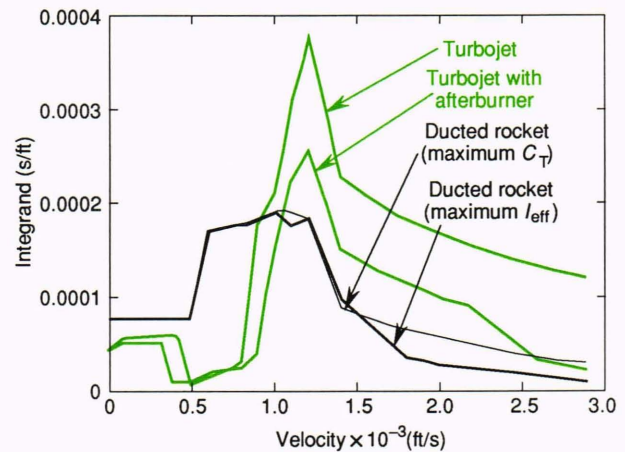


Figure 15. Values of the integrand in Equation 4 for the lower speed range.

Table 3. Fuel required to accelerate to Mach 3 for single-stage-to-orbit vehicles, expressed as a fraction of gross takeoff weight.

Low-speed engine cycle	Vehicle drag		
	Nominal	Nominal without base	Low without base
Turbojet	0.341	0.290	0.236
Turbojet with afterburner	0.212	0.172	0.103
Ducted rocket, maximum I_{eff}	0.202	0.192	0.180
Ducted rocket, maximum C_T	0.228	0.220	0.210

numbers that were examined and for flight along the reference trajectory or along the high trajectory (from Fig. 2). The propellant fractions for the turbojet without afterburning are consistently about 5% of gross takeoff

Table 4. Fuel required to accelerate single-stage-to-orbit vehicles expressed as a fraction of gross takeoff weight.

Low-speed engine cycle	Inlet design M_D	Vehicle drag				
		Nominal		Low without base		
Reference trajectory						
Turbojet	16	0.755	(24.5)*	0.736	(24.5)	0.683
	20	0.767	(24.5)	0.748	(24.5)	0.691
	24	0.784	(19.5)	0.767	(19.5)	0.704
Turbojet with afterburner	16	0.706	(24.5)	0.691	(24.5)	0.626
	20	0.720	(24.5)	0.706	(24.5)	0.636
	24	0.741	(19.5)	0.727	(19.5)	0.651
Ducted rocket, maximum I_{eff}	16	0.703		0.699		0.659
	20	0.717		0.713		0.677
	24	0.738		0.734		0.682
Ducted rocket, maximum C_T	16	0.713		0.709		0.671
	20	0.726		0.723		0.680
	24	0.746		0.743		0.693
High trajectory						
Turbojet	16	0.760	(17.5)	0.741	(17.5)	0.705 (19.5)
	20	0.770	(16.5)	0.753	(16.5)	0.713 (18.5)
	24	0.780	(16.0)	0.772	(16.0)	0.726 (17.5)
Turbojet with afterburner	16	0.712	(17.5)	0.698	(17.5)	0.652 (19.5)
	20	0.724	(16.5)	0.713	(16.5)	0.666 (18.5)
	24	0.735	(16.0)	0.734	(16.0)	0.681 (17.5)
Ducted rocket, maximum I_{eff}	16	0.711	(17.5)	0.705	(17.5)	0.682 (19.5)
	20	0.721	(16.5)	0.719	(16.5)	0.690 (18.5)
	24	0.732	(16.0)	0.740	(16.0)	0.695 (17.5)
Ducted rocket, maximum C_T	16	0.719	(17.5)	0.715	(17.5)	0.694 (19.5)
	20	0.730	(16.5)	0.729	(16.5)	0.687 (18.5)
	24	0.741	(16.0)	0.734	(16.0)	0.700 (17.5)

*Numbers in parentheses are velocities in thousands of feet per second at which adjunct rocket is turned on.

weight higher than with the afterburner and need not be discussed further. Likewise, the maximum C_T ducted rocket requires about 1% more propellant than the maximum I_{eff} case. Thus, the major points can be couched in terms of the remaining two cases. The most profound result is the very small differences in propellant required for the afterburning turbojet and the maximum I_{eff} ducted rocket, except for the cases with very low drag. In fact, the differences are well within the uncertainty bounds on the underlying assumptions that are inherent in the analysis. From a performance perspective, the choice between the two for the SSTO mission could ultimately depend on the amount of propellant reserved for landing. If an operational requirement dictated that the vehicle be able to "touch-and-go," "fly around," and then land, the high specific impulse of the turbojet at low speed at reduced throttle would result in large fuel savings relative to the ducted rocket. Conversely, if pow-

ered fly around is not required, the ducted rocket would be the better choice because the weight of the propulsion system would be considerably less.

The largest weight difference would accrue from the absence of turbomachinery in the ducted rocket. A lesser amount would also be realized for flight along the reference trajectory by eliminating the adjunct rocket. The increase in propellant fraction would only be 0.2% for $M_D = 16$ and 20 and 0.1% for $M_D = 24$. The parenthetical numbers in Table 4 represent the flight velocities in thousands of feet per second at which turning on the adjunct rocket would lead to propellant savings. For the high trajectory, rocket augmentation would be essential for all propulsion cycles, regardless of the vehicle drag characteristics.

With the mass fraction of propellant for the SSTO mission defined, the performance of the same vehicle on a hypersonic cruise mission can be calculated if the lift-

to-drag ratio is specified. The acceleration phase is ended at the desired cruise velocity, and the remainder of the propellant that would have been used to accelerate further is instead used to cruise. The same propellant reserve that is presumed to be adequate for the SSTO mission is assumed in the cruise mission. In general, the altitude at the end of the acceleration phase on the reference trajectory would not be the optimal altitude for cruise, so the first segment of the cruise trajectory would be an altitude change at constant velocity. For this assessment, the small difference in cruise range from that which would accrue from the same propellant expenditure at near-constant altitude is neglected. Indeed, the comparison of cruise performance will avoid the details of the aerodynamic characteristics of the vehicles by simply specifying a constant lift-to-drag ratio L/D , independent of velocity. With this simplification, the cruise portion of the flight is formulated by the well-known Breguet equation, viz., level flight at constant velocity:

Range $\equiv R =$

$$\frac{[T \cos(\alpha + \delta)] \left(\frac{L + T \sin(\alpha + \delta)}{D} \right) \ln \left(\frac{W_i}{W_f - W_p} \right)}{\dot{w}_p [1 - (U_c/U_{S_0})^2]} \quad (19)$$

Here, $U_c = r_0 g_0 / (r_0 + Z_c)$ is the velocity required for a circular orbit of the Earth at an altitude Z_c . For example, taking $Z_c = 150,000$ ft, $g_0 = 32,174$ ft/s², and $r_0 = 3963 \times 5280 = 20.919 \times 10^6$ ft, then $U_c = 25,857$ ft/s. The velocity ratio in the denominator, which is often neglected, becomes quite important at hypersonic speeds.

Figure 16 shows the cruise range for an $L/D = 3$ vehicle powered by the ducted rocket ram-scrumjet engine cycle. Drag during the acceleration phase is the nominal case, with base drag included and $M_D = 16$. From Table 4, the total propellant mass fraction is 0.703. The cruise range curve has some interesting features. For cruise velocities U_c between 16,000 and 25,000 ft/s, the effects of centrifugal lift and higher U_c more than compensate for the smaller propellant fraction and lower specific impulse. Thus, R decreases monotonically with U_c , reaching a minimum of 9044 mi for cruises at 16,000 ft/s. For $4000 \leq U_c \leq 16,000$ ft/s, the balance among the four terms is such that a maximum R_c of 15,880 mi is reached at about $U_c = 9000$ ft/s.

The results show that the SSTO vehicle has a very formidable capability as a cruise vehicle. Indeed, for many possible missions, increased payload potential could be traded for propellant and a corresponding decrease in R . Results also indicate that highly efficient low-speed engine cycles have limited use in the SSTO mission, since the vehicle design has to provide an engine flow path that will permit the ram-scrumjet to operate efficiently over a very broad Mach number range. The consequence is the very small air capture at low speeds, that is, the engine is small compared with the typical supersonic airplane.

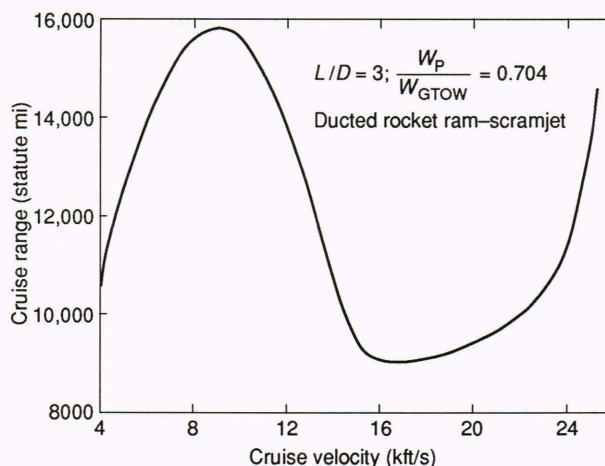


Figure 16. Cruise range capability for single-stage-to-orbit vehicles. (GTOW = gross takeoff weight.)

CONCLUSIONS

At this stage in the iterative conceptual design approach, vehicle lines have been established, flow conditions have been determined for flight along prescribed trajectories, and engine thrusts and fuel flow rates, etc., are known. The rudiments of vehicle aerodynamics have also been examined. Now structural design and materials selection can begin in earnest.

Granting that the results for these tasks can readily be integrated into the design procedure shown in Figure 1, the rationale for the first conceptual vehicle design can be established, and key technical issues can be identified. Preliminary findings from the first iteration in this design process have uncovered a number of challenging problem areas:

1. Volume requirements for the needed hydrogen storage are very difficult to meet.
2. The contribution of the engine thrust vector to the pitching moment of the airplane is very large, which puts stringent requirements on engine placement and alignment to avoid excessive, induced drag.
3. Practical constraints on the amount of variability in the engine geometry and the need to optimize design for hypersonic speeds lead to relatively small engines and a severe thrust-drag pinch point at transonic speeds.
4. Closure (i.e., when required and available weight of propellants are matched) of the vehicle is extremely sensitive to engine component efficiencies, vehicle drag, and structural weights.
5. Good engine performance and structural integrity at Mach numbers above 12 are essential if orbit is to be reached, but ground testing of components is limited under these severe conditions.

Consequently, one cannot unequivocally prove the practicality of an SSTO vehicle. If successful, however, the payoffs are enormous because space will truly be accessible at an affordable cost.

REFERENCES

- ¹Pandolfini, P. P., Billig, F. S., Corpening, G. P., Corda, S., and Friedman, M. A., "Analyzing Hypersonic Engines Using the Ramjet Performance Analy-

F. S. Billig

- sis Code," *APL Tech. Rev.* (limited distribution) 2(1) (in press).
- ²Schetz, J. A., Billig, F. S., and Favin, S., "Modular Analysis of Scramjet Flowfields," *J. Propul. Power* 5(2), 172-180 (1989).
- ³Schetz, J. A., Billig, F. S., and Favin, S., "Numerical Solutions of Scramjet Nozzle Flows," *J. Propul. Power* 3(5), 440-447 (1987).
- ⁴Billig F. S., "Combustion Processes in Supersonic Flow," *J. Propul. Power* 4(3), 209-216 (1988).
- ⁵Small, W. J., Weidner, J. P., and Johnston, P. J., *Scramjet Nozzle Design and Analysis as Applied to a Highly Integrated Hypersonic Research Airplane*, NASA TMX-71972 (Nov 1974).

THE AUTHOR



FREDERICK S. BILLIG received a B.E. (1955) from The Johns Hopkins University and an M.S. (1957) and a Ph.D. (1964) from The University of Maryland, all in mechanical engineering. He joined APL in 1955 and specialized in ramjet propulsion, external burning, and supersonic combustion. He is Associate Department Head and Chief Scientist of the APL Aeronautics Department. Dr. Billig is a member of the U.S. Air Force Scientific Advisory Board and the NASA Space Systems Advisory Committee and is APL program manager for the National AeroSpace Plane project.